Acta Geophysica (2020) 68:1667–1677
https://doi.org/10.1007/s11600-020-00495-0

RESEARCH ARTICLE - APPLIED GEOPHYSICS

Generalisation and improvement of the compact gravity inversion method

Wenwu Zhu[1,2] · Junhuan Peng[1] · Sanming Luo[2] · Xiangang Meng[2] · Jinzhao Liu[2] · Chuandong Zhu[2]

Received: 5 May 2020 / Accepted: 26 September 2020 / Published online: 17 October 2020

Abstract

Compact gravity inversion (CGI) is widely used to invert gravity data following the principle of minimising the volume of the causative body due to its simplicity, high efficiency, and sharp-boundary inversion results. In this study, the compactness weighting function is generalised and the depth weighting function is introduced to CGI to obtain the reweighted CGI (RCGI) method. Although RCGI exhibits better flexibility than CGI, selecting an appropriate compactness factor α and depth weighting function β is difficult, and we design a parameter selection rule to search the proper α and β quantitively. Furthermore, we improve RCGI for boasting superior computational efficiency by gradually eliminating the model blocks that reach the designated boundaries in the iterative algorithm of inversion. This approach is termed the reweighted and element-elimination CGI (REECGI) method. The inversion results show that both RCGI and REECGI result in better inversion accuracy than CGI, and REECGI has higher computational efficiency than RCGI and CGI, which increases with the number of iterations.

Keywords Compact gravity inversion · Inversion theory · Compactness factor · Weighting function · Inversion accuracy · Computational efficiency

Introduction

Gravity inversion is a practical method that has been extensively applied in hydrology, oil and gas exploration, mineral exploration, and geological surveys (Blakely 1995; Chen et al. 2008; Karaoulis et al. 2014; Li and Oldenburg 1998; Mendonca and Silva 1994, 1995; Pilkington 1997, 2009; Portniaguine and Zhdanov 1999; Roland et al. 2013; Zhdanov 2015). Owing to the instability and non-uniqueness of inversion, which is known as the ill-posed problem (Hadamard 1902), it is difficult to obtain inversion information that accurately reflects the real geological conditions below the Earth's surface.

Researchers have made numerous attempts to overcome the ill-posed problem; one solution is to find the appropriate stability function combined with the error function. Constable et al. (1987) and Smith et al. (1991) introduced the minimum norm of the Laplace operator of the model, which can produce a smooth inversion solution; however, this method usually fails to accurately describe the true massive geological structure. Rudin et al. (1992) proposed a method based on total variation (TV) to rebuild noisy and blurred images, but the relative functions are not differentiable at zero. To solve this problem, Acar and Vogel (1994) improved the TV method by introducing a small real number.

However, these methods all attempt to smooth out the inversion results; therefore, they do not represent the actual situation, especially in the case of mineral exploration, where it is desirable to obtain inversion results with sharp boundaries. To obtain sharp-boundary images and overcome the smoothness problem, Last and Kubik (1983) developed the compact gravity inversion (CGI) method based on the minimum area (2D inversion) or volume (3D inversion) of the model blocks, resulting in sharp-boundary inversion images when the blocks are located at shallow depths. This method received widespread attention; however, the effects of non-convergence and concentration near the surface often

Electronic supplementary material The online version of this article (https://doi.org/10.1007/s11600-020-00495-0) contains supplementary material, which is available to authorised users.

✉ Wenwu Zhu
fmccea@sina.com

[1] China University of Geosciences (Beijing), Beijing 100083, China

[2] The First Crust Monitoring and Application Centre, China Earthquake Administration, Tianjin 300180, China

occur during actual gravity inversion. Portniaguine and Zhdanov (1999) proposed a similar approach based on the CGI called the minimum gradient support (MGS) method; however, a similar problem remains (i.e., the near-surface concentration effect). Therefore, the inversion results do not reflect the actual mineral distribution when the model blocks are located at great depths. To obtain accurate inversion results, other scholars used additional a priori information to generalise the CGI method (Barbosa and Silva 1994; Guillen and Menichetti 1984; Silva and Barbosa 2006; Silva et al. 2009, 2011); however, these methods strongly depend on a priori information, including the centre of gravity of the model blocks and the direction of the dyke, which are often unknown in field cases. When there is little a priori information, such interactive and generalised inversion methods are no longer applicable; therefore, Williams (2008) proposed another method of performing inversion without geological constraints. However, this led to new problems such as the need to estimate a large amount of parameters, which is difficult when geologists are not familiar with the local geology and make the procedure more time-consuming.

Considering the advantages and disadvantages of CGI and other methods, this study aims to generalise the CGI method and obtain more reasonable gravity inversion results, while further improving the calculation efficiency. First, we generalise the compactness weighting function of the CGI method and introduce the depth weighting function (Li and Oldenburg 1998) to make the CGI method more flexible for gravity inversion. Second, we propose an approach for quantitatively obtaining the appropriate compactness weighting function factor α and the depth weighting function β. Lastly, we improve the computational efficiency by continuously eliminating the model blocks reaching the bounds, ensuring that the kernel matrix dimensions decreases continuously.

Materials and methods

The density model is assumed to be discretised into several rectangles in two-dimensional (2D) models or rectangular prisms in three-dimensional (3D) models. For simplicity, the inversion method is introduced for a 2D case here; however, the discussion applies equally to the 3D case. It has been established that gravity anomaly data, $\tilde{G}$, has the following relationship with the density model, $\tilde{V}$:

$$\tilde{G} = A\tilde{V}, \tag{1}$$

where $\tilde{G}$ is an adjusted $n \times 1$ vector, $\tilde{V}$ is an $m \times 1$ vector, and A is the kernel matrix, which was defined by Last and Kubik 1983; the dimensions of A are $n \times m$. In Eq. (1), $\tilde{G}$ and A are known values that can be measured or calculated in advance; only $\tilde{V}$ is unknown and needs to be obtained in order to approximate the solution of the actual mineral distribution.

Last and Kubik (1983) used the principle of minimisation of the area (or volume in 3D) of the model to solve Eq. (1), which can be stated as follows:

$$\begin{aligned} &\text{Minimize } Q = \sum_i \tilde{v}_i^2/(\tilde{v}_i^2 + \varepsilon), \quad i = 1, 2, \ldots, m \\ &\text{Subject to} \quad \tilde{G} - A\tilde{V} = 0 \\ &V_{\min} \le \tilde{V} \le V_{\max}, \end{aligned} \tag{2}$$

where $\tilde{v}_i$ is the approximate solution of the ith block, ε is a sufficiently small value [$\approx 10^{-11}$ in the case of Last and Kubik (1983)], and $V_{\min}$ and $V_{\max}$ denote the lower bound vector with the same entries, $v_{\min}$ (a scalar), and the upper-bound vector with the same entries, $v_{\max}$ (a scalar), respectively.

The following characteristic exists for a single block in Q of Eq. (2):

$$q = \lim_{\varepsilon \to 0} \tilde{v}_i^2/(\tilde{v}_i^2 + \varepsilon) = \begin{cases} 0 & \text{for } \tilde{v}_i = 0 \\ 1 & \text{for } \tilde{v}_i \neq 0. \end{cases} \tag{3}$$

According to Eq. (3), the optimal solution of Eq. (2) will be obtained when the number of blocks (= 0) reaches a maximum, which means that the other blocks (≠ 0) are at a minimum. This is why the CGI method follows the principal of the minimum area. In fact, Eq. (2) is a special case as follows:

$$\begin{aligned} &\text{Minimize} F = \sum_i \tilde{v}_i^2/(|\tilde{v}_i^{\alpha} + \varepsilon), \quad \alpha \neq 0 \\ &\text{Subject to } \tilde{G} - A\tilde{V} = 0 \\ &V_{\min} \le \tilde{V} \le V_{\max}, \end{aligned} \tag{4}$$

And the following characteristic exists for a single block in F of Eq. (4):

$$f = \lim_{\varepsilon \to 0} \tilde{v}_i^2/(|\tilde{v}_i|^{\alpha} + \varepsilon) = \begin{cases} 0 & \text{for } \tilde{v}_i = 0 \\ |\tilde{v}_i|^{2-\alpha} & \text{for } \tilde{v}_i \neq 0. \end{cases} \tag{5}$$

Thus, Eqs. (4) and (5) are equal to Eqs. (2) and (3), respectively, when $\alpha = 2$. Equation (5) also follows the same principal as Eq. (3), i.e., the optimal solution is positively correlated to the number of model blocks (= 0) produced in the inversion results. The only difference between Eq. (2) and (4) or Eqs. (3) and (5) is that the constant 2 changes to the variable α. The introduction of this variable provides more flexibility than the CGI method during gravity inversion by allowing variation of α, which is helpful for obtaining better inversion solutions. Actual experiments show that the inversion results are more reasonable when α is a positive real number other than 2.

Next, we continue to follow the approach of Last and Kubik (1983) whereby $1/\left(\left|v_i\right|^{\alpha}+\varepsilon\right)$ in Eq. (4) is considered to be the compactness weighting function, which should be positive. Therefore, $|\bullet|$ is introduced, which represents the absolute value of •, to guarantee that $\left|v_i\right|^{\alpha}$ is always a positive real number (v_i^{α} is probably a negative or an imaginary number when $v_i<0$). Thus, the compactness weighting function has the following matrix form:

$$\tilde{W}=\operatorname{diag}\left(\tilde{w}_i\right), \tag{6}$$

with $\tilde{w}_i=\frac{1}{\left|\tilde{v}_i\right|^{\alpha}+\varepsilon}, \quad i=1,2,\ldots,m, \alpha\neq 0.$

The iteration algorithm is introduced because $\tilde{W}$ is not a constant weighting matrix. In one iteration, $\tilde{W}$ is replaced by the inversion solutions obtained by the last iteration so they become constant matrices in the current iteration, and the iterative procedure is reduced to a classical least L_2-norm problem. The optimal solution of the problem in the kth iteration is as follows (Menke 1989):

$$\tilde{V}^{(k)}=\left[\tilde{W}^{(k-1)}\right]^{-1}A^T\left\{A\left[\tilde{W}^{(k-1)}\right]^{-1}A^T+\mu I\right\}^{-1}\quad \tilde{G},\ k=2,3,\ldots\ldots,\ \mu>0 \tag{7}$$

where $\tilde{W}^{(k-1)}$ represents the compactness weighting function calculated by Eq. (6) in the $(k-1)$th iteration and $\tilde{W}^{(1)}$ is an $m\times m$ identity matrix. μ is a damping factor (Levenberg 1944; Marquardt 1963) used to improve the condition number of the matrices and I is an $n\times n$ identity matrix.

Experiments show that the near-surface concentration effect cannot be overcome when the blocks ($\neq 0$) are located at great depths when only considering the compactness weighting function of the model. Therefore, the depth weighting function (Li and Oldenburg 1998) or the kernel weighting function (Zhdanov 2015) must be added into Eq. (6) and (7) (Ghalehnoee et al. 2017; Rosas-Carbajal et al. 2017). Both these functions have an equivalent effect in overcoming the near-surface concentration effect in the vertical direction (Pilkington 2009); thus, the depth weighting function is used in this study. Accordingly, $\tilde{W}$ changes to a new form:

$$\tilde{W}=\operatorname{diag}\left(\tilde{w}_i\right), \tag{8}$$

with $\tilde{w}_i=\frac{1}{\left(\left|\tilde{v}_i\right|^{\alpha}+\varepsilon\right)z_i^{\beta}}, \alpha>0, \beta\geq 0, z_i>0, i=1,2,\ldots,m,$

where z_i is the depth of the ith model and β is the depth weighting function factor. The reason for the condition of $\alpha>0$ is that the value of $\tilde{v}_i$ obtained in the kth iteration is larger; therefore, the weight of $\tilde{v}_i$ should be larger in the next iteration according to Last and Kubik (1983). If $\alpha<0$, a larger $\tilde{v}_i$ will correspond to a lower weight of $\tilde{v}_i$, which contradicts the earlier assumption; hence, $\alpha>0$. We refer to this CGI method with the depth weighting function as the reweighted compact gravity inversion (RCGI) method because RCGI is equivalent to CGI when $\alpha=2$ and $\beta=0$.

As α and β are variables, determining their appropriate values is another problem. Combining Eq. (4), (7), and (8), we propose two strategies for determining appropriate α and β values in a given interval according to whether the prior model v_i (i = 1, 2, …, m) is known:

$$(\alpha,\beta)=\begin{cases}\arg\min\sum_i\left(\tilde{v}_i-v_i\right)^2, v_i \text{ is known } (a)\\ \arg\min(\gamma\delta), v_i \text{ is unknown } (b)\end{cases}, \tag{9}$$

$\alpha>0, \beta\geq 0, i=1,2,\ldots,m.$ where

$$\begin{cases}\gamma=\text{number of } \tilde{v}_i(\neq 0)\\ \delta=\frac{\tilde{G}-A\tilde{V}_2}{\tilde{G}_2}\end{cases},$$

If the prior model is known, the optimal α and β values are obtained by minimising the sum of the squared residuals between the inversion results $\tilde{v}_i$ and the prior model v_i. Otherwise, the α and β values are obtained by minimising the product of γ (i.e., the number of $\tilde{v}_i(\neq 0)$ that follows the principal of minimum area, allowing the inversion model to be compact) and δ (the relative l_2-norm of the observation data $\tilde{G}$ and the forward result of $\tilde{V}$ that prevent excessively large residuals). The appropriate α and β values for obtaining the optimal solution generally lie within a small interval (i.e., $0.9\leq\alpha\leq 1.2$, $2\leq\beta\leq 6$ in the inversion of synthetic data). Because the inversion results usually cannot be convergent if α and β are too large, as the best interval is unknown at the initial trial, we can instead search for α and β in a slightly larger interval with a slightly larger step to estimate the approximate interval, then gradually narrow down the interval and step to determine the final values of α and β.

Next, we try to improve the already high computational efficiency of the RCGI or CGI methods and obtain REECGI: We find that the weights of the models reaching the lower or upper bounds in the last iteration are all set to a very large value (i.e., 10^{11}); therefore, these blocks can be frozen in the next iteration. In fact, these blocks can be removed in the next iteration because their solutions have been obtained and there is no need to involve them in the calculations any longer. If so, the dimensions of the kernel matrices A and the weighting matrices $\tilde{W}$ in Eq. (7) will be reduced, which then leads to a smaller number of calculations in the next iteration. The specific process for this concept is as follows:

1. Calculate the inversion values using Eqs. (6) and (7);
2. Ascertain whether any inversion results reach the boundary values $v_{\min}$ and $v_{\max}$. If v_i reaches the boundaries:

$$A^{(k)} = \left[A(1,:)^{(k-1)}, A(2,:)^{(k-1)}, \cdots, A(i-1,:)^{(k-1)}, A(i+1,:)^{(k-1)}, \cdots, A(n,:)^{(k-1)} \right],$$
$$\tilde{W}^{(k)} = \mathrm{diag}\left(\tilde{w}_1^{(k-1)}, \tilde{w}_2^{(k-1)}, \ldots, \tilde{w}_{i-1}^{(k-1)}, \tilde{w}_{i+1}^{(k-1)}, \ldots, \tilde{w}_m^{(k-1)} \right), \quad k \geq 2 \tag{10}$$

where $A(i,:)^{(k-1)}$ represents the ith column of A in the $(k-1)$th iteration and $[\bullet]$ represents the matrices constituted by $\bullet$;

3. Repeat step (1) until convergence.

As we can see from Eq. (10) above, the calculation efficiency of REECGI is faster due to the reduction of $A^{(k-1)}$ and $\tilde{W}^{(k-1)}$.

Solving Eq. (7) is an essential step required for the CGI, RCGI, and REECGI methods. Now, we approximately count the smallest reduction of multiplications involved in solving Eq. (7) in one iteration. Assuming that there are t $(0 \leq t \leq m)$ blocks reaching the boundary values in one iteration, the reduction of RCGI has $mn(3m+2n)$ multiplications (this is the same as CGI as it is equal to RCGI when $\alpha = 2$, $\beta = 0$, and the choice of α and β does not change the matrix dimensions for multiplication), whereas REECGI only has $n(m-t)(3(m-t)+2n)$ multiplications. Therefore, the reduction of multiplications for solving Eq. (7) is $nm(3m+2n) - n(m-t)(3(m-t)+2n) = nt(6m-3t+2n)$ in one iteration. This leads to significant time saving when Eq. (9) is used to find the appropriate α and β for more iterations.

Finally, a relative l_2-norm is used to terminate the iteration process in the synthetic data as follows:

$$e_1 = \frac{\tilde{V} - V_2}{V_2}, \tag{11}$$

where $\tilde{V}$ is the recovered model and V is the true model. The threshold and maximum iteration times for the termination of the iteration need to be determined according to the actual situation. Using field data, the difference between two iterations can be considered as the principle for terminating the iteration process as follows:

$$e_2 = \frac{\tilde{V}^{(k)} - \tilde{V}_2^{k-1}}{\tilde{V}_2^{k-1}}, \tag{12}$$

Results and discussion

Inversion of synthetic data

We used the model shown in Fig. 1 to compare the CGI, RCGI, and REECGI methods. The gravity anomaly dataset is obtained by forward modelling with equidistant observations (5 m spacing) in the horizontal direction, and no noise is added into the gravity anomaly data to better compare the three methods and prevent interference caused by noise. The corresponding model blocks are constructed for the same square with a length of 5 m; the example includes three separated bodies with one negative (blue rectangle) and two positive (yellow rectangles) blocks, distributed along the vertical direction. The left and middle models both measure 70 m × 20 m at a depth of 95 m, and the right model is 30 m × 30 m at a depth of 155 m. The lower and upper boundaries are set to − 1000 and 1000 kg m^{-3}, respectively.

First, we use RCGI to conduct the inversion calculations shown in Fig. 2, where α is a fixed value (=2) for comparison with the CGI method. The blue dashed rectangles indicate the locations of the true model blocks. The left column shows the inversion results, and the right shows the relative calculation residuals. In Fig. 2a, b, $\alpha = 2$ and $\beta = 0$, which indicates that the CGI method is used for inversion of the

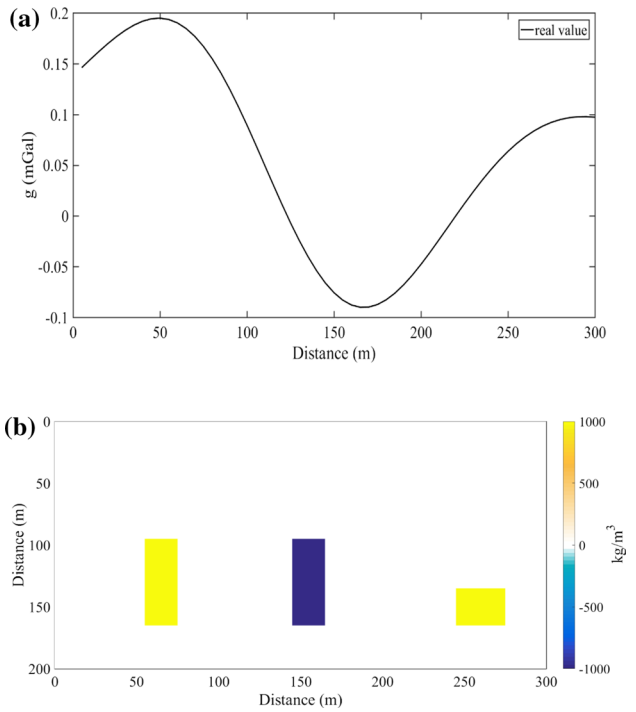

Fig. 1 **a** Actual gravity anomaly data reproduced in **b** by forward modelling of the true model with a positive density value of 1000 kg m^{-3} (yellow rectangles) and a negative value of − 1000 kg m^{-3} (blue rectangle)

synthetic test; i.e., an obvious near-surface concentration of the inversion results exists and the iterative algorithm is convergent. In Fig. 2c, d, $\alpha = 2$ and $\beta = 2.35$. Because β has a positive correlation with the depth of the inversion results, we gradually increase β from zero in order to determine a better value for β, which can improve the accuracy of the inversion results with respect to the real model; this resulted in a β value of 2.35. The location shown in Fig. 2c is closer to the real model than that in Fig. 2a, although the residual error e_1 shown in Fig. 2d is larger than that for CGI shown in Fig. 2b, and the iteration is also convergent. In Fig. 2e, f, the inversion results are no longer convergent, even if β (= 2.40) is only slightly larger than 2.35. Thus, this synthetic test shows that we cannot obtain reasonable inversion results for the case where α is a fixed value (2). In other words, CGI is not applicable in this case.

Figure 2 shows that we cannot obtain good inversion results with a fixed α; therefore, we now use the RCGI and REECGI methods, in which α is also a variable, to obtain better inversion solutions and compare their computational efficiency. The maximum iteration times and e_1 in Eq. (11) are set to 200 and 0.20, respectively, for terminating the iteration algorithm. First, we determine the best α and β in the given interval ($0.9 \le \alpha \le 1.2$, $2 \le \beta \le 6$) for both methods according to Eq. (9a) shown in Fig. 3. In fact, we set a larger interval in the initial test, but the inversion results are too smooth or not convergent when α and β exceed this interval. The left column (Fig. 2a, c) shows the results obtained by

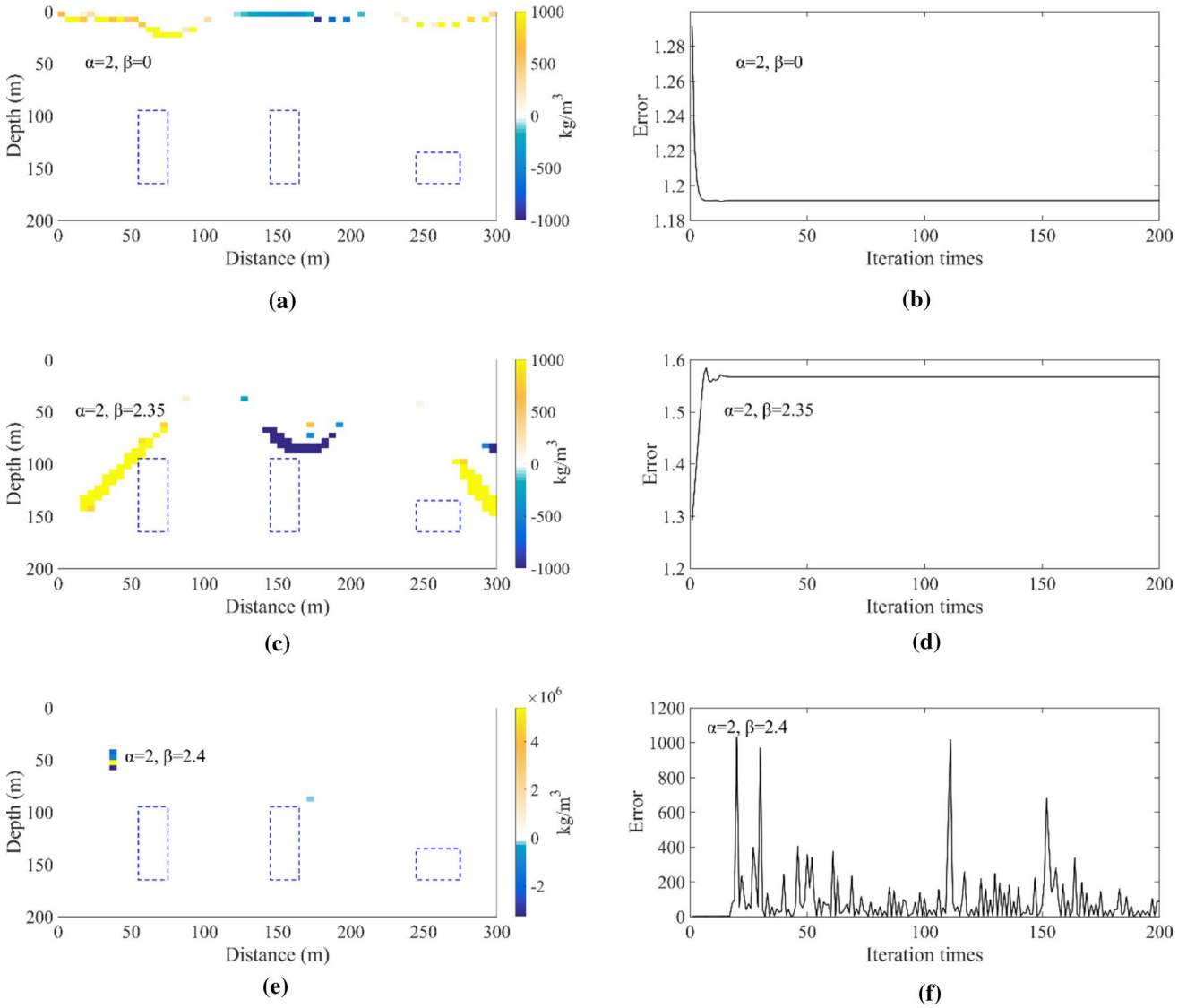

Fig. 2 Inversion results and relative residual errors using the RCGI with a fixed α value of 2 and different β. The blue dashed rectangles in **a**, **c**, and **e** indicate the locations of the true model blocks. The maximum iteration times and e_1 from Eq. (11) are set to 200 and 0.20, respectively, for terminating the iteration algorithm

the RCGI and the right column (Fig. 2b, d) shows the results obtained by the REECGI. The same α and β are obtained by both methods, i.e., $\alpha = 1.0$ and $\beta = 4.0$, as shown in Fig. 2a, b. Moreover, similar inversion results are obtained with the residual errors: 0.2120 and 0.2203 for RCGI and REECGI, respectively. However, there is a certain difference in the computational time between RCGI (697.73 s) and REECGI (650.58 s) when using a 2.2 GHz processor. The saved calculation time of REECGI is approximately 6.7% compared to RCGI.

Inversion of field data

In this section, we apply the CGI, RCGI, and REECGI methods to the inversion of gravity anomaly field data measured in an iron ore mine at Qian'an, Hebei Province, China. The iron ore is predominantly located in the strata of the Archean Santunying Formation with a background density of 2670 kg m^{-3}. There are three tectonic boundaries shown in Fig. 4: F1, F2, and F3. F1 is composed of north-west F1–1, F1–2, and F1–3 tectonic boundaries, F2 is composed of south-west F2–1 and F2–2 tectonic boundaries, and F3 is a north-east stratigraphic lithology interface. We follow the principle of cutting structures to design three profiles, P201, P202, and P203, placed 200 m from each other.

The CG-5 relative gravimeter (No. 1095) produced by Scintrex in Canada is used to measure the gravity anomaly with a measurement accuracy of better than 5 μGal. The field data is further processed by normal field, Bouguer, and terrain corrections. As shown in Fig. 4, the high gravity anomaly area is predominantly distributed to the west of F3, whereas the low gravity anomaly area is to the east. The background density information is removed from the gravity measurements by forward modelling.

According to existing geological data shown in Fig. 5 (Fig. 5a shows the 3D model structure of the ore body in the study area, Figs. 5b–d shows the 2D model structure beneath profiles P201, P202, and P203, respectively), the composition of the ore minerals is as follows. The dominant mineral type is hematite, followed by a small amount of martite with a band-shaped structure, represented as yellow polygons in the figure. Both ore minerals are treated as having the same density and the corresponding residual density is 660 kg m^{-3}. In addition, some low-density rock masses exist that constitute a broken complex (residual density: − 470 kg m^{-3}), represented as dark blue polygons, as well as sedimentary rocks (residual density: − 70 kg m^{-3}), which are represented as light blue polygons. Based on the available data, the entire inversion area is set to 1200 m × 1000 m, and the corresponding

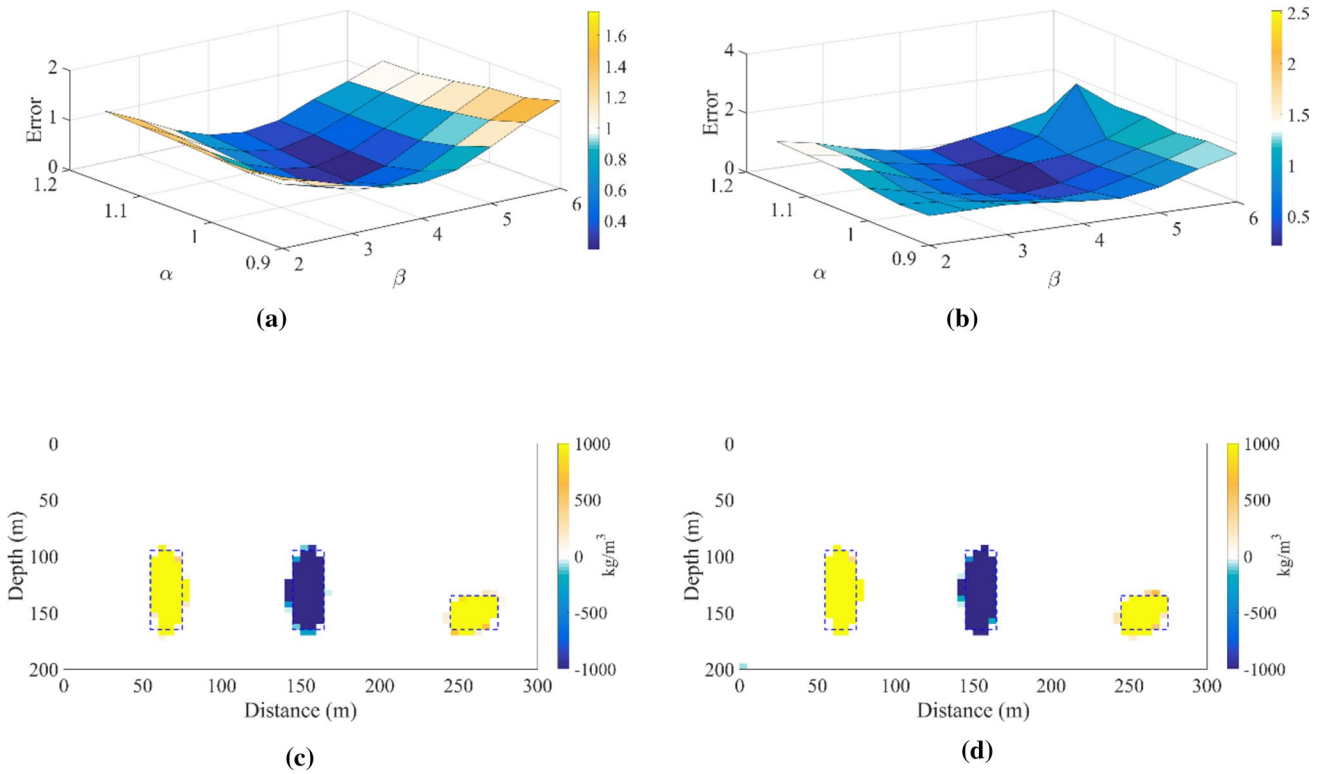

Fig. 3 Optimal α and β values determined by **a** RCGI and **b** REECGI. The same α and β values ($\alpha = 1.0$, $\beta = 4.0$) are obtained by both methods. Inversion results from **c** RCGI and **d** REECGI

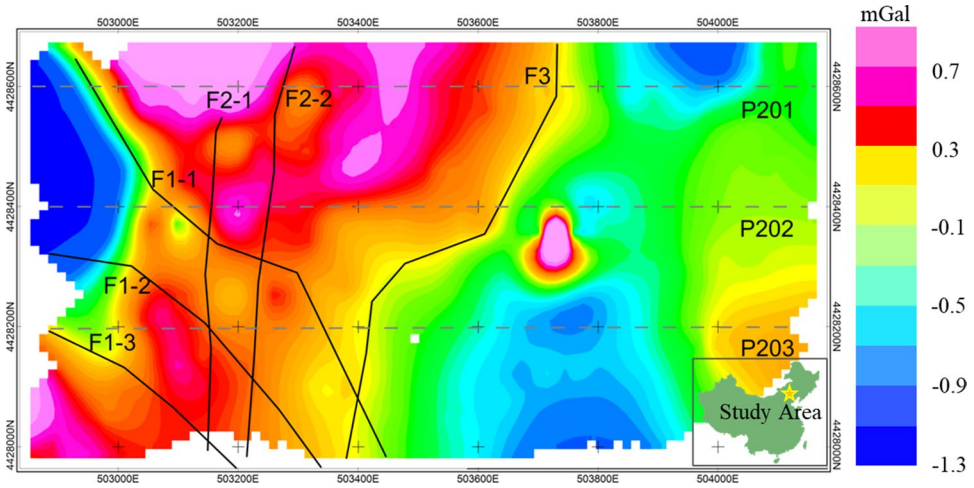

Fig. 4 Study area of an iron ore mine in Qian'an, Hebei Province, China. There are three tectonic boundaries: F1 (composed of north-west F1–1, F1–2, and F1–3), F2 (composed of south-west F2–1 and F2–2), and F3 (north-east stratigraphic lithology interface). The three profiles P201, P202, and P203 are located 200 m from each other

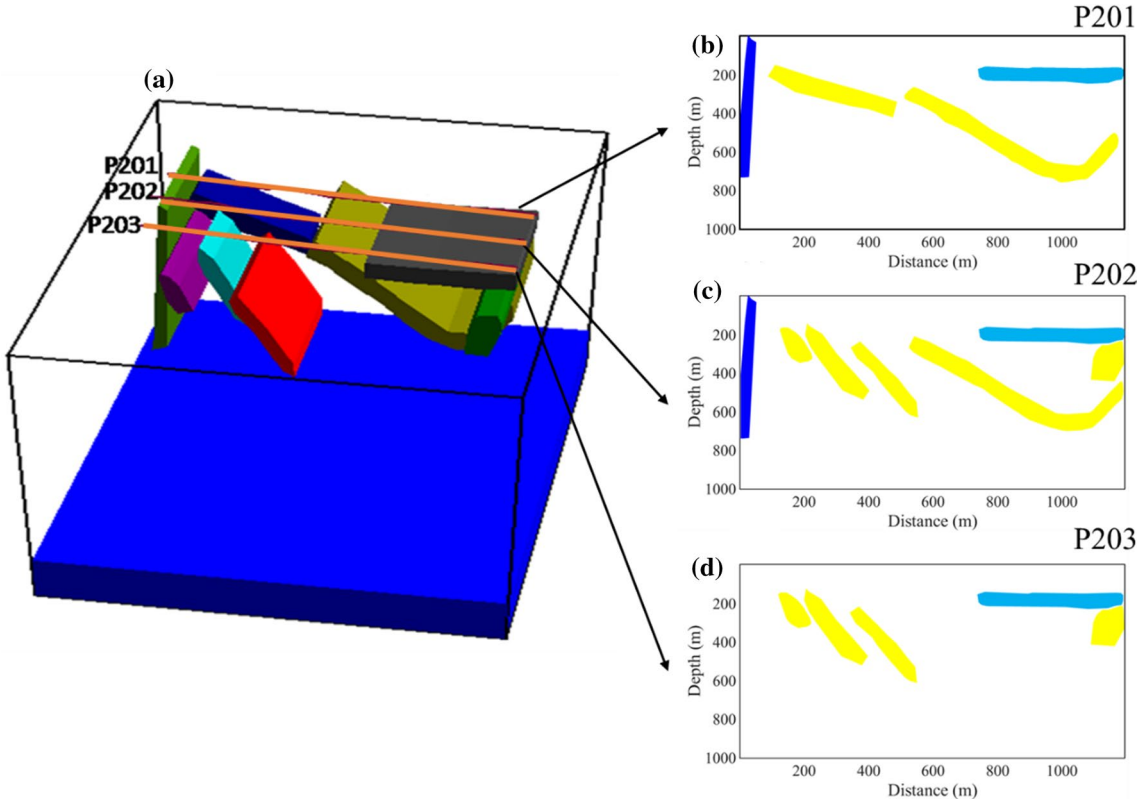

Fig. 5 Mineral distribution beneath the three profiles, P201, P202, and P203: **a** Overall distribution of minerals. Simplified mineral distribution beneath **b** P201; **c** P202; and **d** P203. Three types of minerals are shown: hematite (residual density 630 kg m^{-3}) represented by yellow polygons, broken complexes (residual density − 470 kg m^{-3}) in dark blue polygons, and sedimentary rocks in light blue polygons

model blocks consist of a 120 m × 100 m grid with dimensions of 10 m × 10 m in the horizontal and vertical directions, respectively.

Now, we conduct inversions of the three profiles using CGI, RCGI, and REECGI methods. The CGI method with fixed α (= 2) and β (= 0) is first used to confirm its unsuitability at great depths in the inversion area. As we can see from Fig. 6, the inversion results of all three profiles show significant near-surface concentration effects, although they are compact (Fig. 6a–c, e) and the data residuals are small (Fig. 6b, d, f).

As CGI is deemed unsuitable for this study, we apply RCGI and REECGI for the three profiles. The best choice of α and β should naturally be considered; thus, the step sizes are set to 0.01, and the corresponding α and β values of the three profiles obtained by Eq. (9b) are shown in

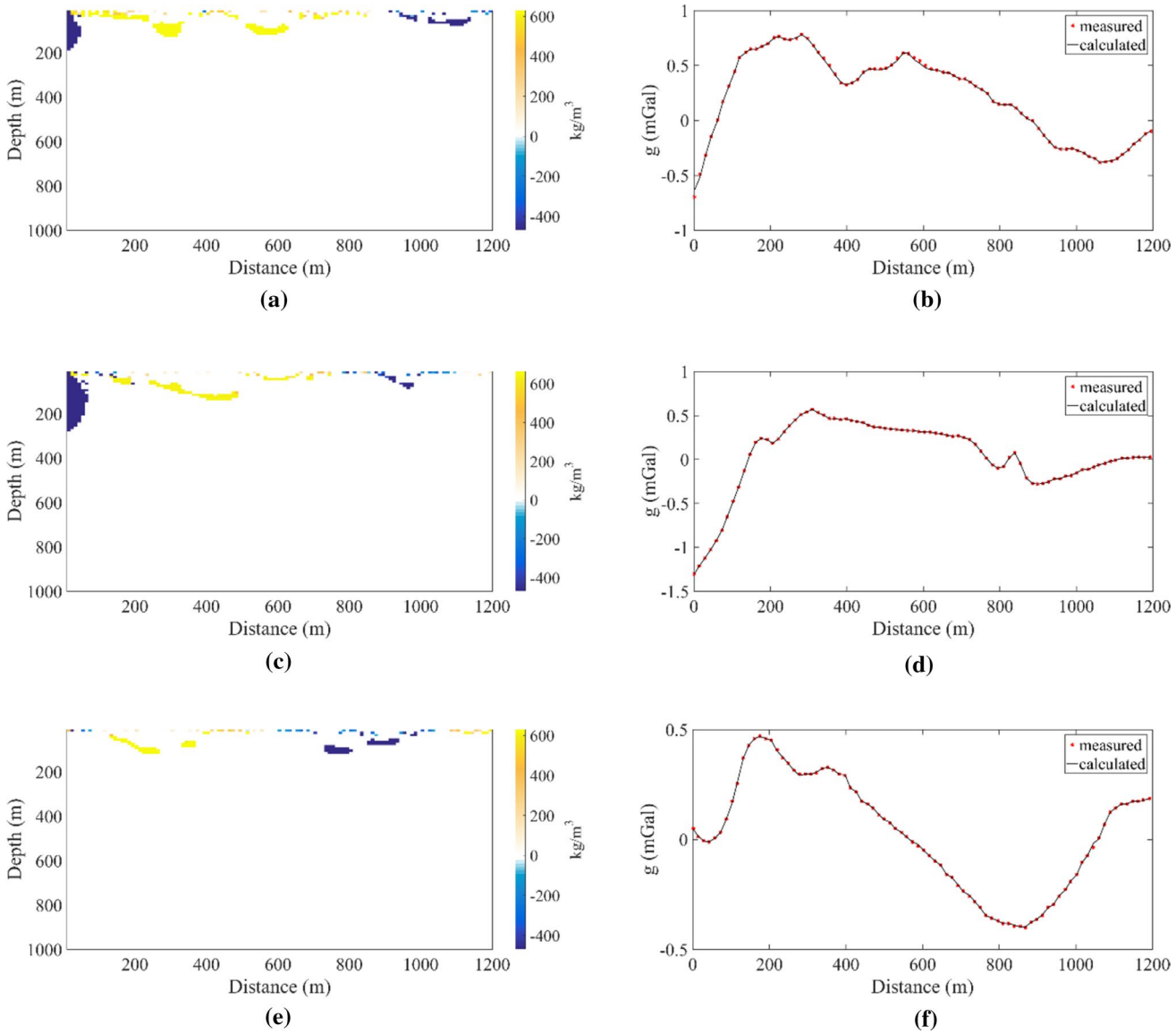

Fig. 6 Inversion results (left) and corresponding data misfits (right) determined by CGI for **a**, **b** P201; **c**, **d** P202; and **e**, **f** P203. Near-surface concentration effects are observed in the inversion results of all three profiles

Table 1. As the data fitting results are good, we do not show the data fitting charts for both methods as shown in Fig. 6b, d, f. The inversion results of the three profiles obtained with the appropriate α and β values using the two methods are shown in Fig. 7 (results in the left column are obtained by RCGI and those in the right are obtained by REECGI). Both methods yield almost the same results for P201, P202, and P203, as shown in Fig. 7a–f, in which the hematite, broken complex, and sedimentary rocks are shown as yellow, dark blue, and light blue polygons, respectively.

Table 1 Optimal α and β values of RCGI and REECGI methods used for the inversion of three gravity anomaly profiles, P201, P202, and P203. Both step sizes are set to 0.01 for determining α and β values within the same interval

Method	P201		P202		P203	
	α	β	α	β	α	β
RCGI	1.60	1.70	1.49	1.13	1.70	1.70
REECGI						

For P201, compared to the prior geological information shown in Fig. 5b, the inversion results of the broken complex are closer to the actual situation than those of hematite and sedimentary rocks. The worst inversion solution is obtained where the hematite (positive density) and the sedimentary rocks (negative density) are vertically overlapped. Only a small amount of sedimentary rocks and hematite is obtained, as shown in Fig. 7a, b. For P202, compared to the results shown in Fig. 5c, the left broken complex and the shallow hematite are obtained relatively accurately, whereas the very deep minerals, especially when overlapped with sedimentary rocks, are difficult to obtain, as seen from Fig. 7c, d. For P203, compared to results shown in Fig. 5d, the hematite and sedimentary rocks in the middle of Fig. 7e, f are obtained relatively accurately, unlike those at other locations.

Finally, we test the computational times of the RCGI and REECGI methods using P201, as shown in Fig. 8. In order to observe the calculation efficiency of the two methods more intuitively, the number of iterations are set to 100, 300, 600, and 1000 times, respectively. According to Fig. 8, the computational time of REECGI is lower than that of RCGI, and the time saved becomes more significant as the number of iterations increases.

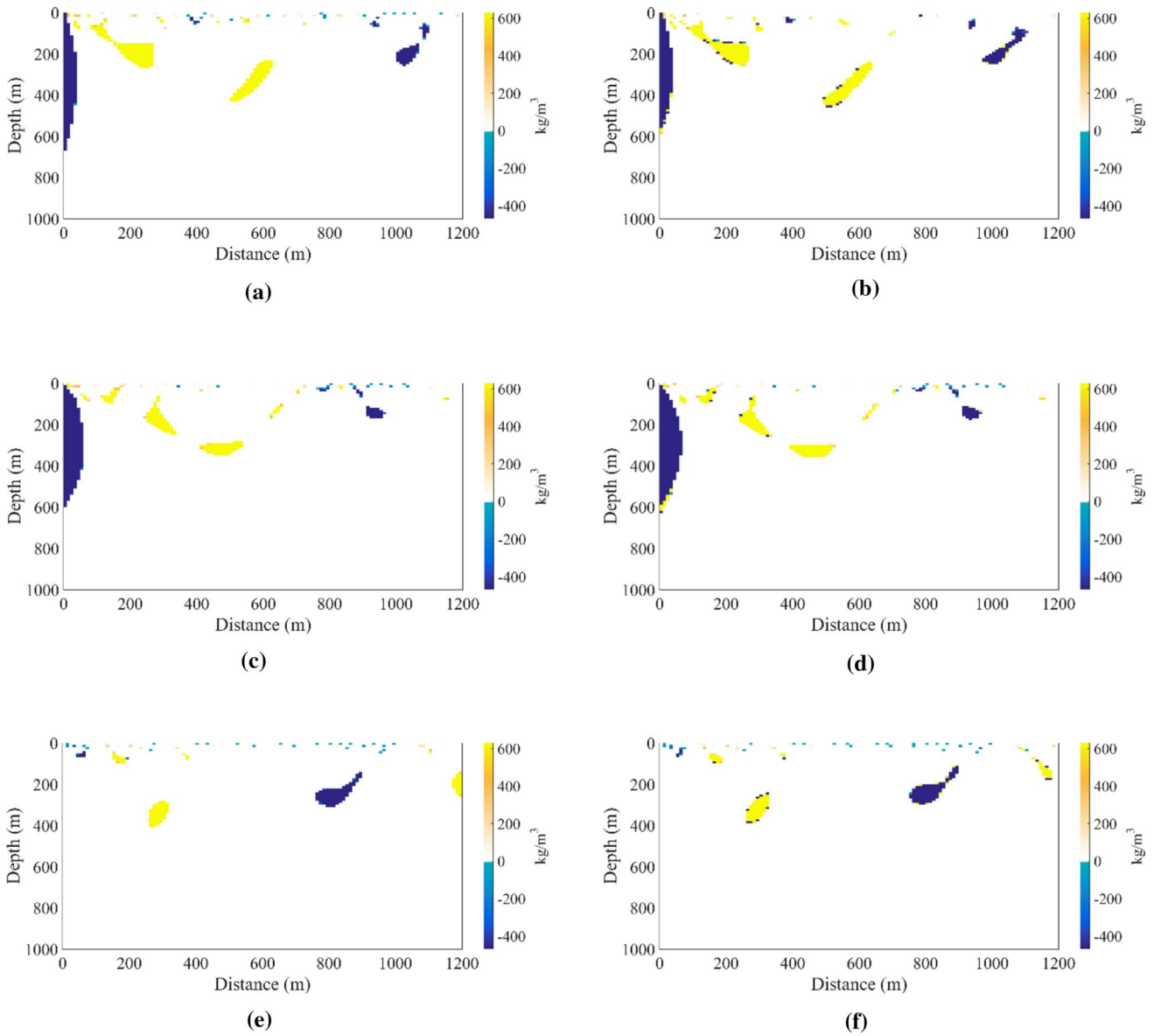

Fig. 7 Inversion results of profiles P201, P202, and P203 by RCGI and REECGI. The left column shows the inversion results of RCGI for **a** P201, **c** P202, and **e** P203. The right column shows the inversion results of REECGI for **b** P201, **d** P202, and **f** P203. The inversion results of the two methods are almost the same

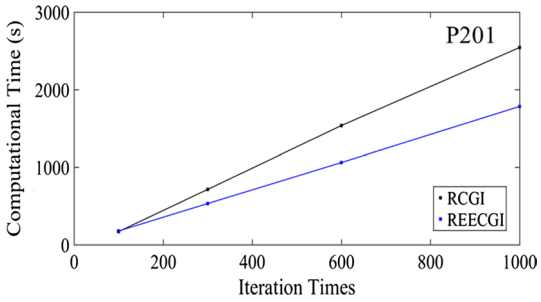

Fig. 8 Comparison of the computational time required by RCGI and REECGI methods using profile P201. The black and blue lines represent the computational time of RCGI and REECGI, respectively. REECGI is more efficient that RCGI, and the efficiency increases with the number of iterations

Conclusion

We developed the RCGI method to ensure high flexibility for gravity anomaly inversion, especially for compact mineral models located at great depths, by generalising the classic CGI method. We then developed the REECGI method by improving the RCGI method to have higher computational efficiency. In addition, we proposed a quantitative method for determining the two key parameters (the compactness weighting factor α and the depth weighing factor β) required to obtain the optimal solution of RCGI or REECGI methods. Synthetic and field tests both indicate that RCGI and REECGI result in more accurate inversions of positive and negative model blocks than CGI, and that REECGI is more efficient than RCGI. The REECGI method can be easily run on a computer in only a few seconds, and can be applied to the inversion of any gravity data to obtain more acceptable resolution in the vertical direction.

Acknowledgements We would like to thank Prof. Shi Chen of the Institute of Geophysics, China Earthquake Administration for providing field data as well as specific guidance. We also thank Prof. Bofeng Guo of Tianjin University for offering constructive comments and editing the manuscript. Further, we would like to thank Editage (www.editage.cn) for English language editing.

Author contributions Conceptualisation was done by JP and SL; Methodology was done by WZ; Software was done by WZ; Validation was done by JL and CZ; Resources was done by XM; Data Curation was done by WZ; Writing-Original Draft Preparation was done by WZ; Writing-Review and Editing were done by JL and CZ; Visualisation was done by WZ; Project Administration was done by XM; Funding Acquisition was done by XM. All authors have read and approved the final version of the manuscript.

Funding This research was funded by the National Key R & D Program of China, Grant Nos. 2018YFC1503606 and 2017YFC1500501.

Data Availability Applicable.

Compliance with ethical standards

Conflict of interest The authors declare no conflict of interest.

Code availability Applicable.

References

Acar R, Vogel CR (1994) Analysis of total variation penalty methods. Inverse Prob 10:1217–1229
Barbosa VCF, Silva JBC (1994) Gen Compact Gravity Invers Geophys 59(1):57–68
Blakely RJ (1995) Potential theory in gravity and magnetic applications. Cambridge University Press, Cambridge
Chen S, Zhang J, Shi YL (2008) Gravity inversion using the frequency characteristics of the density distribution. Appl Geophys 5(2):99–106
Constable SC, Parker RC, Constable GG (1987) Occam's inversion: a practical algorithm for generating smooth models from EM sounding data. Geophys 52:289–300
Ghalehnoee MH, Ansari A, Ghorbani A (2017) Improving compact gravity inversion using new weighting functions. Geophys J Int 28(1):546–560
Guillen A, Menichetti V (1984) Gravity and magnetic inversion with minimization of a specific functional. Geophys 49:1354–1360
Hadamard J (1902) Sur les problèmes aux derivées partielles et leur signification physique. Princeton Univ Bull 13: 49–52. Reprinted in his Oeuvres, Centre Nat Rech Sci, Paris, 3:1099–1105
Karaoulis K, Revil A, Minsley B et al (2014) Time-lapse gravity inversion with an active time constraint. Geophys J Int 196:748–759
Last BJ, Kubik K (1983) Compact gravity invers Geophys 34:65–74
Levenberg K (1944) A method for the solution of certain nonlinear problems in least squares. Q Appl Math 2:164–168
Li YG, Oldenburg DW (1998) 3-D inversion of gravity data. Geophys 63(1):109–119
Marquardt DW (1963) An algorithm for least squares estimation of nonlinear parameters. SIAM J 11:431–441
Mendonca CA, Silva JBC (1994) The equivalent data concept applied to the interpolation of potential field data. Geophys 59(5):722–732
Mendonca CA, Silva JBC (1995) Interpolation of potential field data by equivalent layer and minimum curvature: a comparative analysis. Geophys 60(2):399–407
Menke W (1989) Geophysical data analysis: discrete inverse theory, Revised edn. Academic Press, Cambridge
Pilkington M (1997) 3-D magnetic imaging using conjugate gradients. Geophys 62:1132–1142
Pilkington M (2009) 3D magnetic data-space inversion with sparseness constraints. Geophys 74(1):L7–L15
Portniaguine O, Zhdanov MS (1999) Focusing Geophys Invers Images Geophys 64(3):874–887
Roland M, Vadim M, Dimitri K et al (2013) Gravity inversion using wavelet-based compression on parallel hybrid CPU/GPU systems: application to southwest Ghana. Geophys J Int 195:1594–1619
Rosas-Carbajal M, Jourde K, Marteau J et al (2017) Three-dimensional density structure of La Soufrière de Guadeloupe lava dome from simultaneous muon radiographies and gravity data. Geophys Res Lett 44(13):6743–6751
Rudin LI, Osher S, Fatemi E (1992) Nonlinear total variation-based noise removal algorithms. Phys D 60:259–268
Silva FJS, Barbosa CF, Silva JBC (2009) 3D gravity inversion through an adaptive-learning procedure. Geophys 74(3):I9–I21

Silva FJS, Barbosa CF, Silva JBC (2011) Adaptive learning 3D gravity inversion for salt-body imaging. Geophys 76(3):I49–I57

Silva JBC, Barbosa VCF (2006) Interactive gravity inversion. Geophysics 71(1):J1–J9

Smith RT, Zoltani CK, Klem GJ, Coleman MW (1991) Reconstruction of the tomographic images from sparse data sets by a new finite element maximum entropy approach. Appl Opt 30:573–582

Williams NC (2008) Geologically-constrained UBC-GIF gravity and magnetic inversion with examples from the Agnew-Wiluna greenstone belt, Western Australia. PhD thesis, The University of British Colombia, Faculty of Geophysics

Zhdanov MS (2015) Inverse theory and applications in geophysics. Elsevier, Amsterdam